

# A Leaf-Level Dataset for Soybean–Cotton Detection and Segmentation

Thiago H. Segreto<sup>1,\*</sup>, Juliano Negri<sup>1</sup>, Paulo H Polegato<sup>1</sup>, João Manoel Herrera Pinheiro<sup>1</sup>, Ricardo Godoy<sup>1</sup>, and Marcelo Becker<sup>1</sup>

<sup>1</sup>Mechanical Engineering Department, São Carlos School of Engineering, University of São Paulo, São Carlos 13566-590, SP, Brazil

\*corresponding author(s): Thiago H. Segreto (thiago.segreto.silva@alumni.usp.br)

## ABSTRACT

Soybean and cotton are major drivers of many countries' agricultural sectors, offering substantial economic returns but also facing persistent challenges from volunteer plants and weeds that hamper sustainable management. Effectively controlling volunteer plants and weeds demands advanced recognition strategies that can identify these amidst complex crop canopies. While deep learning methods have demonstrated promising results for leaf-level detection and segmentation, existing datasets often fail to capture the complexity of real-world agricultural fields. To address this, we collected 640 high-resolution images from a commercial farm spanning multiple growth stages, weed pressures, and lighting variations. Each image is annotated at the leaf-instance level, with 7,221 soybean and 5,190 cotton leaves labeled via bounding boxes and segmentation masks, capturing overlapping foliage, small leaf size, and morphological similarities. We validate this dataset using YOLOv11, demonstrating state-of-the-art performance in accurately identifying and segmenting overlapping foliage. Our publicly available dataset supports advanced applications such as selective herbicide spraying and pest monitoring and can foster more robust, data-driven strategies for soybean–cotton management.

## Background & Summary

Soybean (*Glycine max* (L.) Merr.) and cotton (*Gossypium hirsutum* L.) are among the most significant crops in many countries' agriculture, playing a key role in Brazil's national economy<sup>1,2</sup>. The integration of these crops into rotational systems, such as soybean–cotton or soybean–corn, enhances soil health and fertility while mitigating agronomic risks commonly associated with monoculture practices<sup>3</sup>. However, this rotation introduces specific management challenges, particularly the emergence of volunteer plants, soybean or cotton shoots that germinate from residual seeds of previous seasons. These compete directly with the main crop for critical resources, including water, light, and nutrients, and can serve as hosts for pests such as the cotton boll weevil (*Anthonomus grandis*), posing a significant threat to crop yield and necessitating rigorous management strategies<sup>4,5</sup>.

Traditional management of weeds or unwanted volunteer plants predominantly relies on blanket herbicide spraying. Although this approach is often effective, its overuse has led to significant concerns, including the emergence of herbicide-resistant weed populations, rising input costs, and adverse environmental impacts<sup>6,7</sup>. In parallel, the management of residual cotton stalks remains critical for effective pest control, especially in disrupting the life cycle of the cotton boll weevil. This practice is not only agronomically essential but also legally mandated in regions where the sanitary void policy enforces the eradication of volunteer plants to prevent pest proliferation<sup>8,9</sup>. These challenges corroborate the critical need for innovative and precise control strategies capable of accurately distinguishing between volunteer plants, active crops, and weeds, thereby enabling more targeted and sustainable interventions<sup>5,10</sup>.

Recent computer vision and deep learning advances have introduced robust solutions for automating plant identification, contributing to more sustainable agricultural practices. Convolutional Neural Networks (CNNs) and Transformer-based vision architectures, particularly when applied to semantic segmentation and object detection, can classify foliage at multiple scales, distinguishing crops and weeds even in complex field conditions<sup>11–13</sup>. While semantic segmentation excels in pixel-level detail, facilitating tasks such as green cover estimation, leaf area indexing, and early disease detection<sup>11</sup>, bounding-box detection offers a more computationally efficient alternative for large-scale mapping and plant identification. When employed together, these methods provide both broad spatial context and refined morphological analyses<sup>14</sup>. Indeed, prior studies have successfully employed segmentation and detection to differentiate weeds from crops such as carrot<sup>15</sup>, cotton<sup>16</sup>, and sugarcane<sup>17</sup>. However, many existing datasets still focus on a single task (often weed detection) and lack comprehensive annotation formats, e.g., semantic masks without instance labels or only bounding boxes, limiting the ability of deep learning models to manage overlapping crops and diverse weed pressures<sup>18</sup>.



**Figure 1.** Ground-truth annotations include detection bounding boxes, shown in the first row, and segmentation masks, shown in the second row.

Despite the importance of robust training data, comprehensive real-world agricultural datasets, particularly those supporting instance segmentation, remain scarce. For example, the Moving Fields Weed Dataset<sup>19</sup> provides numerous annotations but is constrained to controlled indoor environments. In contrast, Champ et al.<sup>20</sup> captured outdoor scenes yet included only about 700 labels per target crop (2,489 total annotations), while the Leaf Segmentation and Counting Challenge<sup>21</sup> offers just 284 labeled instances. Many existing resources also focus on narrow applications, such as disease detection or single-species classification, thus limiting the adaptability of models to diverse field conditions<sup>22</sup>. Although datasets like *DeepWeeds* address multiple weed species<sup>11</sup>, they often lack the multi-modal annotations required for complex tasks, including precise herbicide application and morphological trait analysis<sup>23</sup>.

To meet this need, in this paper, we introduce a soybean–cotton leaf detection and segmentation dataset developed under realistic field conditions on a farm in São Paulo, Brazil. The dataset features images across different growth stages, environmental lighting conditions, and degrees of weed pressure, which are known requirements to make deep learning applications robust in the outdoor uncontrolled scenario<sup>24,25</sup>. Each image is meticulously annotated with both soybean and cotton leaves, even when partial occlusions or overlapping foliage present significant identification challenges. By accommodating both object detection and semantic segmentation formats, as shown in Fig. 1, this resource enables advanced applications: (1) mapping the locations soybean or cotton leaves for targeted herbicide spraying, (2) distinguishing the active crop from surrounding weeds through relatively simple computational filters, and (3) extracting precise morphological features for phenotyping or disease surveillance<sup>11,22</sup>.

## Methods

**Image Acquisition.** All images were collected on a commercial farm in Jaboticabal (São Paulo, Brazil) over a ten-week period. Field personnel captured approximately 70 images weekly, from morning to late afternoon (roughly 6 am to 6 pm) to capture a diverse range of light conditions. This yielded a total of 700 images. However, an automated quality-control procedure discarded 60 low-quality or near-duplicate samples, leaving 640 high-quality photos.

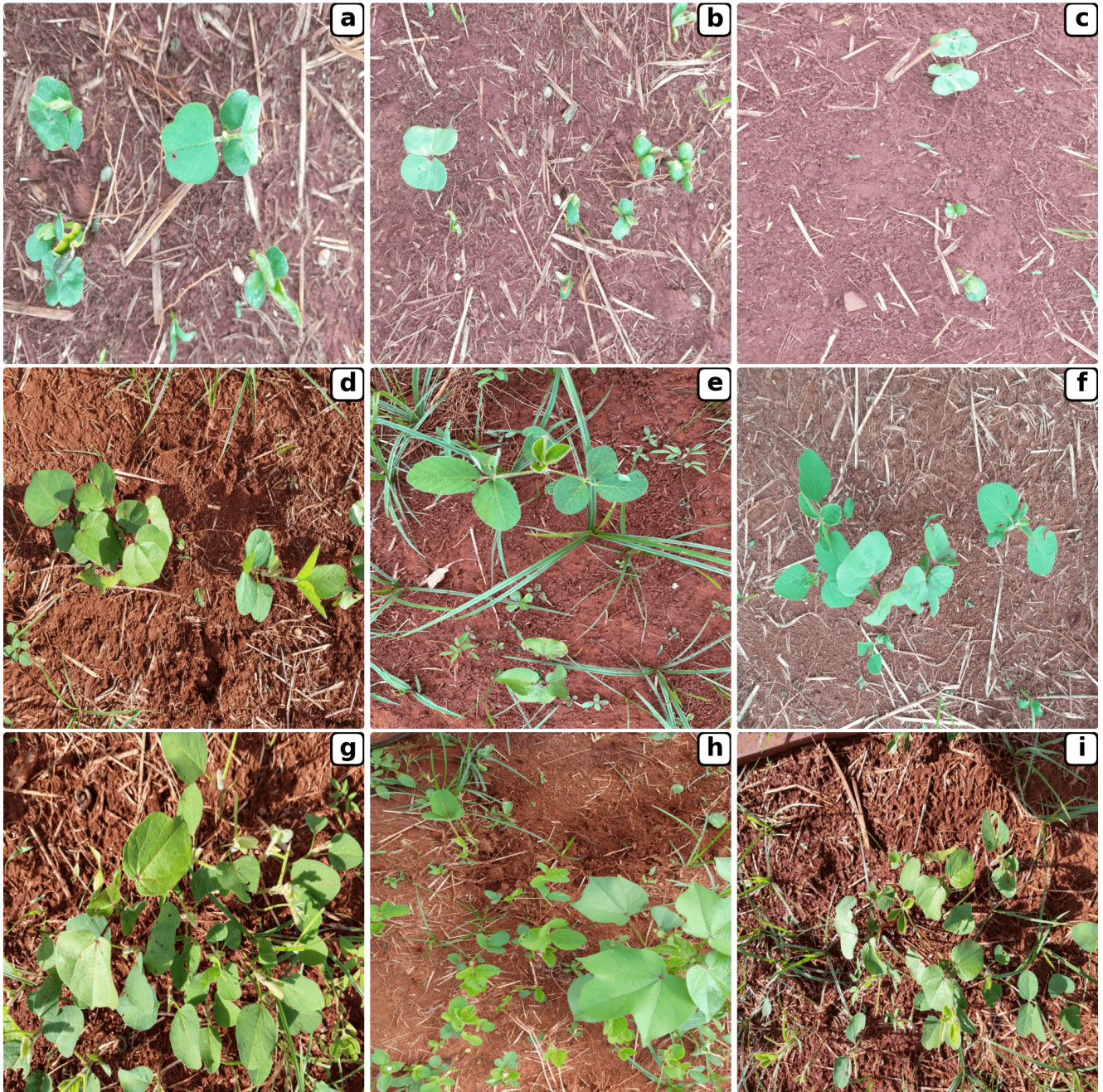


**Figure 2.** Growth stage variations in soybean and cotton fields. A  $3 \times 3$  grid of raw images illustrates early (a–c), middle (d–f), and dense (g–i) canopy stages. In the early stage (1–3 weeks), sparse foliage and minimal leaf overlap simplify segmentation but offer limited complexity. The middle stage (4–7 weeks) introduces denser coverage, partial occlusions, and moderate weed presence. The dense stage (8–10 weeks) exhibits substantial leaf overlap, shading, and varied leaf sizes, posing increased challenges for both detection and segmentation.

Images were taken at roughly knee-to waist-level using multiple smartphone cameras, all set to  $1600 \times 1200$  resolution. Despite the consistent output resolution, the differences in camera models and vantage points were intentional, reflecting the diversity of real-world acquisition scenarios. Soybean fields ranged from emergence (VE) to near full seed (R6), while cotton fields progressed from emergence to a pre-boll stage, collectively providing a broad spectrum of phenotypic appearances. Notably, no herbicides were applied during the collection period, allowing various weed species to remain in the background. This choice ensured a realistic context where the target crops coexisted with non-target vegetation. To further illustrate the

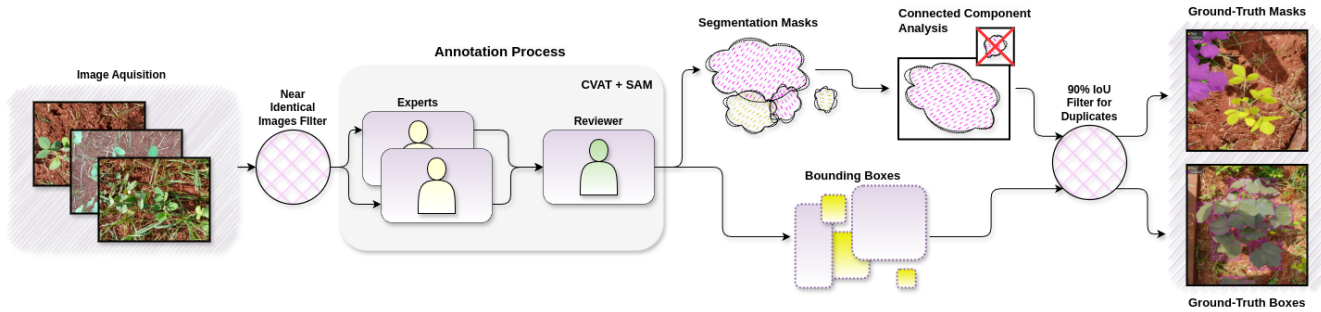


**Figure 3.** Illustration of the dataset creation and annotation workflow. Field images are first acquired under near-vertical perspectives and filtered to remove near-identical samples. Experts and a reviewer then generate initial segmentation masks and bounding boxes in CVAT, assisted by the SAM. Connected component analysis eliminates small “blob” artifacts in the masks, and any duplicate labels are merged using a 90% IoU filter. The final output includes precise ground-truth masks and bounding boxes for soybean and cotton leaves.

progression of crop development across the ten-week span, Fig. 2 presents a 3×3 grid of representative raw images capturing early, middle, and dense foliage stages in both soybean and cotton fields.

**Annotation Process.** Leaf-level annotations were generated using the Computer Vision Annotation Tool (CVAT)<sup>26</sup>, aided by the Segment Anything Model (SAM)<sup>27</sup>. Two experts specializing in soybean and cotton identification performed the core labeling, with a third reviewer overseeing consistency checks. Any leaf recognizable as soybean or cotton, despite potential occlusions or slight blur, was annotated with an instance segmentation mask and a corresponding bounding box to support both semantic segmentation and object detection tasks.

**Annotation Criteria.**

- **Inclusion:** Every visible soybean or cotton leaf was labeled, regardless of size, health, or overlap with other foliage, provided experts reached a consensus on its class.
- **Exclusion:** Weeds, soil, and other background elements were *not* annotated (though they remain unaltered in the images). Leaves too obscured for definite class determination were also excluded.

This procedure yielded 12,411 annotated leaves. 7,221 soybean and 5,190 cotton, and given the large volume of annotated soybean and cotton leaves, occasional human labeling errors led to duplicate or near-duplicate entries. To mitigate this, we filtered duplicate annotations by applying a 90% Intersection over Union (IoU) threshold, effectively removing redundant labels that could undermine data integrity. In parallel, we discovered random “pixel blob” artifacts introduced by the Segment Anything Model (SAM). Although often subtle, these blobs could obscure true leaf boundaries and were more noticeable on blurrier masks. Leveraging OpenCV<sup>28</sup>, we performed connected component analysis to detect and remove small, disconnected blobs, thereby refining the precision of each segmentation mask. Fig. 3 showcases the entire dataset creation pipeline.

**Table 1.** Summary of Dataset Composition

Parameter	Value	Notes
<b>Total Images</b>	640	After discarding 60 low-quality samples
<b>Resolution</b>	1600 × 1200	Multiple smartphone cameras
<b>Soybean Leaves</b>	7,221	From emergence (VE) to near R6
<b>Cotton Leaves</b>	5,290	From emergence to pre-boll stage
<b>Annotations</b>	Masks + bounding boxes	CVAT with SAM

Table 1 provides a concise overview of the final dataset, including the number of annotated leaves for each crop, imaging resolution, and annotation formats. Because no herbicides were applied, weeds and other background elements remained in the fields, offering a realistic context for assessing algorithmic robustness. The deliberate variability in viewing angles, lighting conditions, and growth stages aims to challenge both segmentation and detection algorithms, while the presence of diverse weeds provides an additional layer of complexity. In this regard, this dataset enables tasks ranging from basic crop/weed discrimination to advanced leaf-level trait extraction.

## Data Records

All data described in this study are publicly available under a *CC\_BY\_4.0* license at:

<https://figshare.com/articles/dataset/SoyCotton-Leafs/28466636?file=52552745>.

The repository contains a single top-level folder named `SoyCotton`, which is organized into two subfolders:

- `images`: This folder contains all of the RGB images used in the dataset. Each file is saved in PNG format at a resolution of  $1600 \times 1200$  pixels.
- `annotations`: This folder holds the `coco.json` file, which follows the standard COCO format and provides both bounding-box and instance-segmentation labels for soybean and cotton leaves.

Within the `annotations` file, each image is referenced by a unique identifier, and every annotated leaf is associated with its corresponding bounding box coordinates and polygonal mask. Users can leverage common COCO-compatible libraries or toolkits to parse, visualize, and modify these annotations as needed.

## Technical Validation

This section outlines the procedures and results used to validate both object detection and instance segmentation tasks using the YOLOv11 model<sup>29</sup>. We selected YOLOv11 for its robust real-time performance and unified framework that supports both bounding-box detection and instance segmentation, and its single-stage, lightweight architecture simplifies deployment and training, while still achieving accuracy on par or superior to other state-of-the-art models<sup>29,30</sup>, such as RT-DETR<sup>31</sup>. After a thorough data inspection and label corrections, we optimized hyperparameters for this custom dataset. We then assessed the tuned model via five-fold cross-validation<sup>27</sup> and a data ablation study to evaluate predictive outcomes as the dataset size increased.

**Dataset Splits.** All data splits described below were shuffled and stratified by soybean and cotton class ratios using `scikit-learn`<sup>32</sup>, ensuring representative distributions across training, validation, and test sets.

- **Hyperparameter Tuning (80–10–10):** The dataset was divided into 80% for training, 10% for validation, and 10% for a hold-out test set. This split provided a balanced foundation for tuning model parameters and performing initial performance checks.
- **Five-Fold Performance Analysis (80–20):** From the same 80% training portion, we applied a five-fold cross-validation strategy to further evaluate model stability. Each fold used 80% of the training set for training and 20% for validation, mitigating overfitting to a single split.
- **Data Ablation Study (90–10):** A separate experiment allocated a fixed 10% of the dataset for testing, while the remaining 90% was subdivided into ten equal chunks (each 9% of the full data). Models were trained incrementally on 10%, 20%, ..., up to 90% of the data to analyze how increasing dataset size influenced detection and segmentation outcomes.

**Classification Metrics: Precision, Recall, and F1-Score.** For evaluating the classification performance of object detection and segmentation, we use precision, recall, and the F1-score, defined as follows:

$$\text{Precision} = \frac{TP}{TP + FP}, \quad \text{Recall} = \frac{TP}{TP + FN}, \quad \text{F1} = 2 \times \frac{\text{Precision} \times \text{Recall}}{\text{Precision} + \text{Recall}}$$

*Precision* quantifies the accuracy of positive predictions, representing the proportion of predicted instances (e.g., detected objects or segmented regions) that are correct. A high precision indicates fewer false positives, meaning the model avoids over-predicting. *Recall*, also known as sensitivity, measures the model's ability to detect all actual instances, expressing the fraction of ground-truth objects or regions successfully identified. High recall implies fewer missed detections (i.e., fewer false negatives). The *F1-score* is the harmonic mean of precision and recall, providing a single metric that balances the trade-off between the two. It is particularly useful when the model's performance must account for both false positives and false negatives equally, favoring neither over-detection nor under-detection.

**Intersection over Union (IoU).** IoU is a fundamental metric used to assess the spatial overlap between a predicted bounding box or mask and its corresponding ground-truth annotation. It is defined as:

$$\text{IoU} = \frac{\text{Area of Intersection}}{\text{Area of Union}},$$

where the "Area of Intersection" is the overlapping region between the predicted and ground-truth areas, and the "Area of Union" is the total area spanned by both, excluding double-counting of the intersection. IoU ranges from 0 to 1, with 1 indicating a perfect match and 0 indicating no overlap. In object detection and segmentation, a prediction is typically classified as a true positive if its IoU with the ground truth exceeds a specified threshold (e.g., 0.5). IoU serves as the foundation for computing mean Average Precision (mAP), as it determines the correctness of each prediction.

**Mean Average Precision at IoU=0.5 (mAP<sub>50</sub>).** The mAP<sub>50</sub> metric assesses performance at an IoU threshold of 0.5. For each class  $c$ , predictions are ranked by confidence scores, and precision and recall are computed at each rank. The Average Precision (AP) for class  $c$  is the area under the Precision–Recall curve, often approximated using the all-point interpolation method:

$$\text{AP}_{50}^c = \sum_{k=1}^{N_c} (\text{Recall}_k^c - \text{Recall}_{k-1}^c) \cdot \max_{j \geq k} \text{Precision}_j^c,$$

where  $N_c$  is the number of predictions for class  $c$ ,  $\text{Recall}_k^c$  and  $\text{Precision}_k^c$  are the recall and precision at rank  $k$ , and  $\text{Recall}_0^c = 0$ . The mAP<sub>50</sub> is then the mean of AP across all  $C$  classes:

$$\text{mAP}_{50} = \frac{1}{C} \sum_{c=1}^C \text{AP}_{50}^c.$$

An IoU threshold of 0.5 implies that a prediction is correct if it overlaps at least 50% with the ground truth, making mAP<sub>50</sub> a relatively lenient measure of localization accuracy.

**Mean Average Precision at IoU=0.5:0.95 (mAP<sub>50–95</sub>).** The mAP<sub>50–95</sub> metric extends mAP<sub>50</sub> by averaging mAP scores over IoU thresholds from 0.5 to 0.95 in steps of 0.05 (i.e.,  $T = \{0.5, 0.55, 0.6, \dots, 0.95\}$ , totaling 10 thresholds). For each threshold  $t \in T$  and class  $c$ ,  $\text{AP}_t^c$  is computed as above, adjusting the TP/FP/FN classification based on  $t$ . The mAP<sub>50–95</sub> is then:

$$\text{mAP}_{50-95} = \frac{1}{|T|} \sum_{t \in T} \left( \frac{1}{C} \sum_{c=1}^C \text{AP}_t^c \right) = \frac{1}{10} \sum_{t=0.5}^{0.95, \Delta t=0.05} \text{mAP}_t,$$

where  $\text{mAP}_t = \frac{1}{C} \sum_{c=1}^C \text{AP}_t^c$  is the mAP at threshold  $t$ , and  $|T| = 10$ . This metric rigorously evaluates localization precision, as higher IoU thresholds (e.g., 0.95) demand near-perfect overlap, making mAP<sub>50–95</sub> a robust indicator of model quality across varying levels of spatial accuracy.

**Hyperparameter Optimization.** Soybean and cotton leaves share similar shapes and colors, making them hard to distinguish from each other and from common weeds in real-world scenarios. Depending on leaf age and the camera viewpoint, leaves can appear very small, further complicating detection and segmentation tasks<sup>33</sup>. To address these challenges, we optimized the medium-sized YOLOv11 model using a variant of the *Tree-structured Parzen Estimator (TPE)*<sup>34</sup> for multiple objective metrics, a Bayesian approach known for effective hyperparameter tuning in diverse deep learning applications<sup>35</sup>.

We aimed to produce hyperparameter settings suitable for both detection and segmentation. Thus, we applied the *Multiobjective TPE (MOTPE)*<sup>36</sup> via Optuna<sup>37</sup> to optimize F1-score (capturing classification performance) and mAP<sub>50–95</sub> (measuring spatial accuracy) simultaneously. To expedite the search process, we used distributed training with ClearML<sup>38</sup> across multiple workers, coupled with the Adam optimizer<sup>39</sup>. As a result, the TPE-based searches provided an approximate 4–5% lift in mAP<sub>50–95</sub> and a 2–3% boost in F1-score for both tasks.

Table 2 presents the 11 hyperparameters most critical to convergence, regularization, and data augmentation. Each parameter differs from its default setting to maximize performance gains under the challenging conditions posed by highly similar crop foliage.

**Five-Fold Cross-Validation Performance on YOLOv11 Medium.** Following the hyperparameter search, the YOLOv11 medium model was subjected to a five-fold cross-validation for both detection (bounding boxes) and segmentation (instance masks). Tables 3 and 4 summarize the overall precision (P), recall (R), F1-score, mAP<sub>50</sub>, and mAP<sub>50–95</sub> across folds for detection and segmentation, respectively. Each row includes the mean and standard deviation over the five folds, offering insight into performance variability.

**Table 2.** Optimal hyperparameters derived via MOTPE for the YOLOv11 medium-sized model, optimized for F1 and mAP<sub>50-95</sub>. Each column indicates the final best value found for *Detection* vs. *Segmentation*, differing from default settings.

Hyperparameter	Detection	Segmentation
Initial Learning Rate (LR0)	0.0001	0.0046
Learning Rate Factor (LRF)	0.095	0.097
Momentum (MOMENTUM)	0.92	0.80
Weight Decay (WEIGHT_DECAY)	0.0001	0.0003
Box Loss Gain (BOX)	6.0	6.5
Classification Loss Gain (CLS)	1.0	0.1
Mixup Augmentation (MIXUP)	0.3	0.1
DFL Loss Gain (DFL)	0.3	2.3
Scale Augmentation (SCALE)	0.9	0.6
Perspective Augmentation (PERSPECTIVE)	0.001	0.0
Translate Augmentation (TRANSLATE)	0.1	0.0

**Table 3.** Five-fold cross-validation results for YOLOv11 medium on **detection**. P, R, and F1 are reported as mean  $\pm$  standard deviation, along with mAP<sub>50</sub> and mAP<sub>50-95</sub>.

Category	P	R	F1	mAP <sub>50</sub>	mAP <sub>50-95</sub>
All	0.883 $\pm$ 0.005	0.835 $\pm$ 0.005	0.858 $\pm$ 0.001	0.905 $\pm$ 0.001	0.812 $\pm$ 0.003
Soy	0.858 $\pm$ 0.009	0.803 $\pm$ 0.009	0.830 $\pm$ 0.001	0.877 $\pm$ 0.001	0.770 $\pm$ 0.003
Cotton	0.907 $\pm$ 0.004	0.867 $\pm$ 0.007	0.887 $\pm$ 0.003	0.934 $\pm$ 0.002	0.854 $\pm$ 0.004

**Table 4.** Five-fold cross-validation results for YOLOv11 medium on **segmentation**.

Category	P	R	F1	mAP <sub>50</sub>	mAP <sub>50-95</sub>
All	0.864 $\pm$ 0.010	0.804 $\pm$ 0.009	0.833 $\pm$ 0.006	0.892 $\pm$ 0.004	0.786 $\pm$ 0.005
Soy	0.829 $\pm$ 0.020	0.774 $\pm$ 0.009	0.800 $\pm$ 0.008	0.863 $\pm$ 0.006	0.748 $\pm$ 0.004
Cotton	0.899 $\pm$ 0.014	0.834 $\pm$ 0.015	0.865 $\pm$ 0.009	0.923 $\pm$ 0.004	0.824 $\pm$ 0.007

Figures 4 and 5 provide complementary visualizations. Figure 4 highlights the model’s detection predictions alongside ground-truth bounding boxes, showing its capacity to localize soybean and cotton leaves accurately. Meanwhile, Figure 5 compares ground-truth segmentation masks with the model’s predicted masks, revealing how well YOLOv11 medium delineates leaf boundaries at the pixel level. The numbers associated with the bounding boxes and segmentation masks in the prediction image represent the classification confidence values.

Detection yields slightly higher precision, recall, and F1-score than segmentation, due to the simpler task of predicting bounding boxes compared to the complexity of pixel-wise annotation. As seen in Tables 3 and 4, the “All” category achieves a mean precision of 0.883 for detection versus 0.864 for segmentation. This gap is also mirrored in recall (0.835 vs. 0.804) and F1-score (0.858 vs. 0.833). Such differences are expected, as delineating precise boundaries in densely populated images often demands higher variability in training samples and more intricate feature extraction.

In terms of crop-specific performance, cotton exhibits marginally higher metrics than soybean across both tasks. For detection, cotton’s precision of 0.907 and recall of 0.867 surpass soybean’s 0.858 and 0.803, respectively; the trend persists in segmentation metrics as well. These differences may be rooted in leaf morphology, as cotton leaves present more distinct lobes and shape cues, making them easier to distinguish in occluded or overlapping scenarios. Soybean leaves, by contrast, appear more uniform, potentially leading to a higher incidence of missed detections or imprecise segmentation where occlusion is severe.



**Figure 4.** Detection comparison. The left image (GT) depicts ground-truth bounding boxes for soybean (yellow) and cotton (purple). The right image (Pred) shows the model's bounding-box outputs with confidence scores (blue).



**Figure 5.** Segmentation comparison. The left image (GT) illustrates manual annotations, with soybean leaves in yellow and cotton leaves in purple, whereas the right image (Pred) presents the model-generated segmentation masks.

Lastly, Fig. 6 showcases predictions at different growth stages: early, mid, and dense canopies. In the early phase, with fewer overlapping leaves, bounding boxes and segmentation masks tend to align closely with ground truth. However, as foliage density increases (e.g., near canopy closure), performance on both tasks degrades due to heightened occlusion and partial leaf coverage. For robust field-level applications, these findings emphasize the importance of training on images representing diverse plant densities and stages.

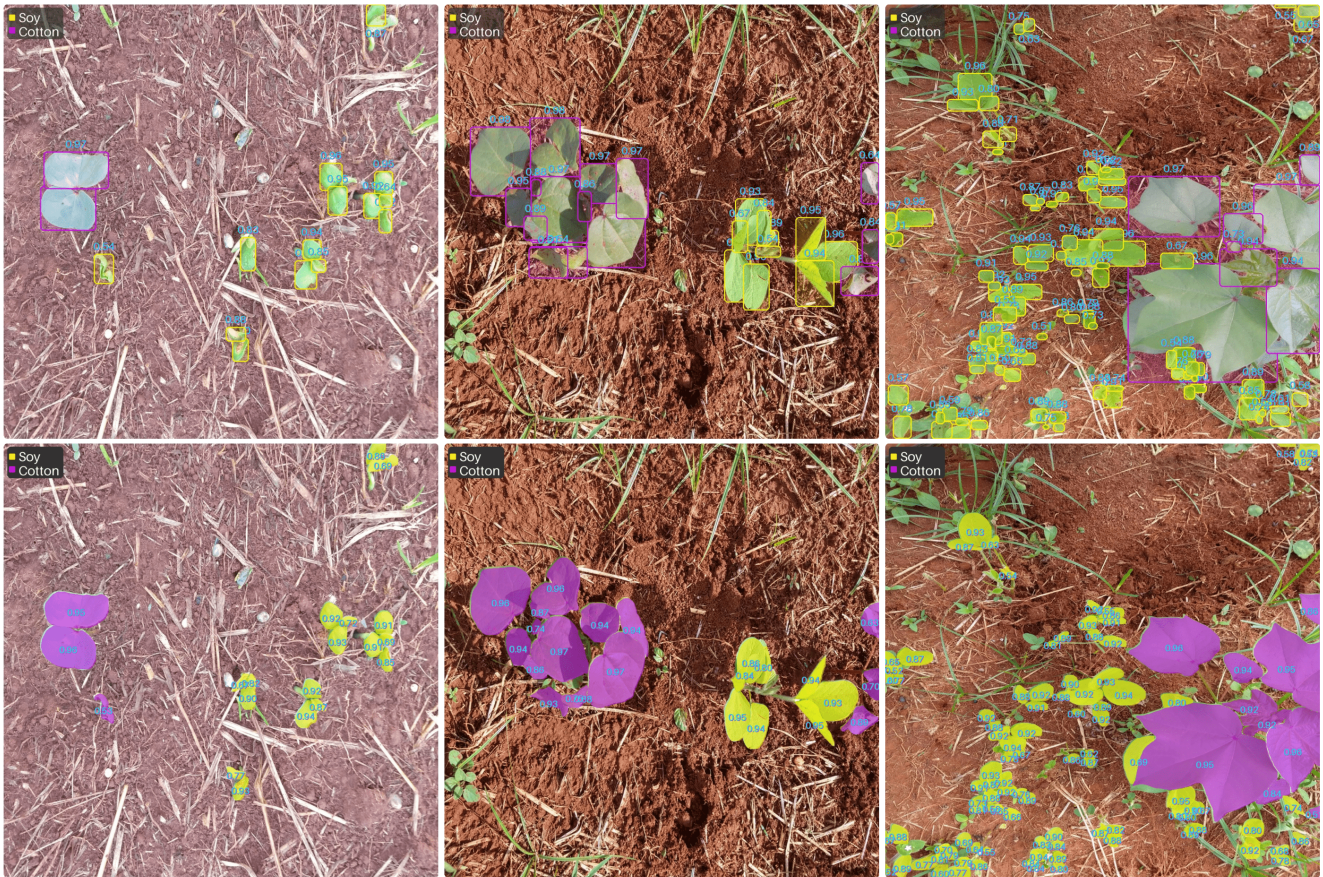


**Figure 6.** Detection and segmentation across soybean and cotton growth stages. This  $2 \times 3$  grid displays YOLOv11m outputs: the top row shows predicted bounding boxes, and the bottom row presents corresponding segmentation masks for early, mid, and dense leaf maturity (left to right). Early-stage predictions exhibit clear leaf separation, while dense-stage outputs reflect challenges posed by occlusions and overlapping foliage.

**Data Ablation Analysis.** To investigate the impact of dataset size on model performance, we conducted a data ablation analysis using three variants of the YOLOv11 model—small (S), medium (M), and large (X)—trained on incrementally increasing portions of the dataset. The dataset, comprising annotated cotton and soybean objects, was divided using a 90–10 split: 90% of the data was allocated for training and partitioned into equal increments, while the remaining 10% was reserved as a fixed test set to ensure consistent evaluation across all experiments. The training increments were stratified and randomly sampled to preserve class balance at each ablation step.

Figure 7 illustrates the relationship between  $mAP_{50-95}$  and the number of annotated objects for each model–task combination. An exponential curve was fitted to these data points via `curve_fit` in `scipy`<sup>40</sup> to capture the saturation trend better as dataset size increases. We note that detection tasks tend to plateau around 7,000 objects, whereas segmentation tasks often continue to improve until reaching approximately 9,000–11,000 objects. This discrepancy indicates that bounding-box detection saturates earlier, while pixel-level segmentation benefits from additional annotations, likely due to its higher granularity and complexity.

Table 5 provides a mock-up for quantifying marginal improvements in  $mAP_{50-95}$  at key annotation thresholds. Although all model variants (S, M, and X) show strong early gains, the rate of improvement drops markedly once the plateau region is reached. Notably, the YOLOv11-X model, with 56.9 million parameters, retains an edge over smaller variants, especially in segmentation tasks, suggesting that a higher capacity model can better leverage a larger dataset.

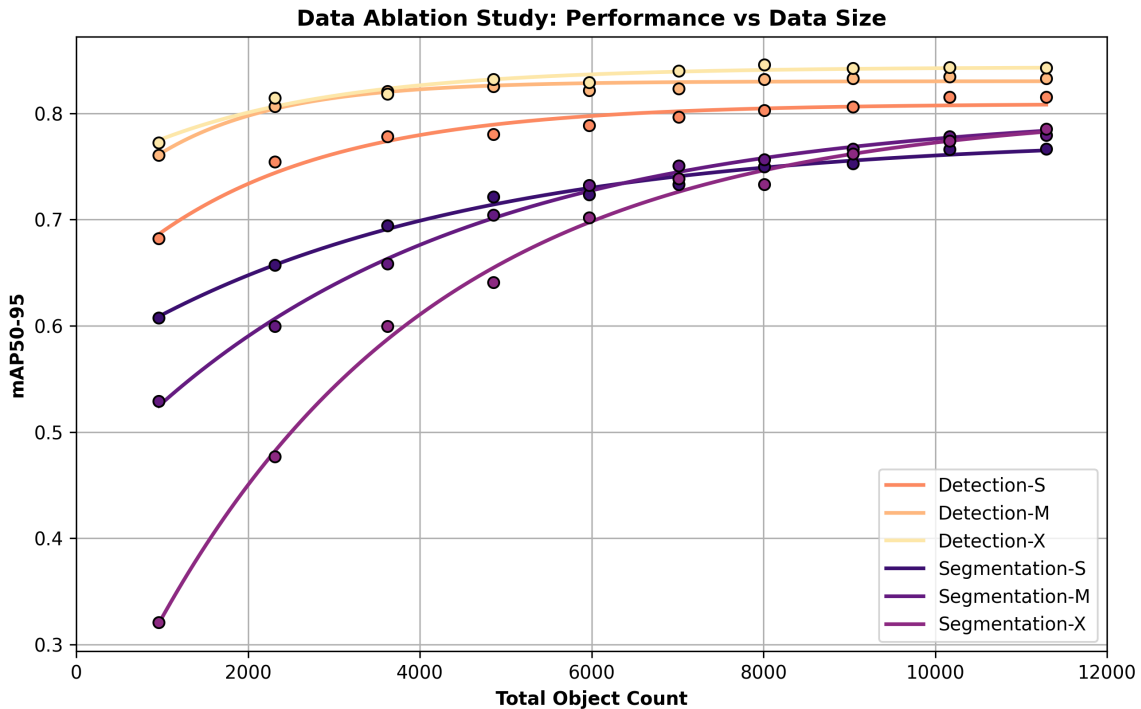


**Figure 7.** Effect of dataset size on YOLOv11 performance for detection (yellow for S, orange for M, red for X) and segmentation (pink for S, purple for M, dark blue for X). The x-axis indicates the total number of annotated objects used in training, and the y-axis shows mAP<sub>50-95</sub>. Detection appears to plateau near 7,000 objects, while segmentation gains persist until roughly 9,000–11,000 objects. An exponential curve is fitted to the data (not shown here explicitly) to illustrate the saturation effect.

**Table 5.** Marginal improvements in detection and segmentation performance at three data-size milestones for the YOLOv11 medium model.

Annotated Objects	Detection mAP <sub>50-95</sub>	Segmentation mAP <sub>50-95</sub>	Detection Gain	Seg. Gain
9,042	83.3	76.6	+0.1	+1.0
10,167	83.5	77.8	+0.2	+1.2
11,293	83.3	78.0	-0.2	+0.1

This analysis highlights two practical considerations:

- **Early vs. Late Plateau:** If the primary goal is rapid bounding-box detection, annotating beyond 7,000 objects yields only marginal gains. Conversely, segmentation requires fine-grained annotations and benefits from additional data up to around 9,000–11,000 objects.
- **Model Complexity:** Larger architectures (e.g., YOLOv11-X) show slightly more extended improvements, implying higher capacity models can extract nuanced features from additional training data. However, the YOLOv11-M model provides a good trade-off between accuracy and computational efficiency.

Future work might investigate how advanced data augmentation or alternative labeling methods could further lift performance, especially once the model begins to plateau. As such, beyond these observed thresholds, increasing annotation volume alone may not guarantee significant gains; refinements in data quality, model architecture, or training strategy could be more impactful.

## Code availability

All scripts used to reproduce the dataset splits, as well as convert them to the YOLO format, are available at [SoyCotton-Repository](#). This repository contains instructions in the ReadMe for replicating our experimental results and testing configurations. For users who prefer custom data manipulation, we recommend referring to the COCO annotation format guidelines to integrate these annotations into alternative pipelines.

## Acknowledgements

This work was supported by the *Fundação de Apoio à Física e à Química* (FAFQ) and funded by *Instituto Matogrossense do Algodão* (IMAmT) and the *Cooperativa Mista de Desenvolvimento do Agronegócio* (COMDEAGRO) under grants EMBRAPPI PIFS-2111.0043.

## Author contributions statement

T.H.S.: Conceptualization, Methodology, Data Curation, Validation, Writing - J.N.: Data Curation, Validation, Writing & Editing - P.H.P.: Methodology, Data Curation, Writing & Editing - J.M.H.P.: Methodology, Validation - R.G.: Methodology, Writing & Editing - M.B.: Project Administration, Resources, Supervision - All authors reviewed the manuscript.

## Competing interests

The authors declare no competing interests.

## References

1. Companhia Nacional de Abastecimento (Conab). Primeira estimativa para safra de grãos 2024/25 indica produção de 322,47 milhões de toneladas (2024). Accessed: 28/11/2024.
2. Food and Agriculture Organization of the United Nations. *World Food and Agriculture – Statistical Yearbook 2023* (FAO, Rome, 2023).
3. Embrapa Algodão. *Cultura do Algodão no Cerrado* (Embrapa, Brasília, Brasil, 2017).
4. Agrolink. Como manejar as tigueras no algodoeiro (2023). Accessed: 28/11/2024.
5. Instituto Mato-Grossense do Algodão. Circular técnica n 41: Destruição de soqueiras do algodoeiro (2019). Accessed: 28/11/2024.
6. Cavenaghi, A. L., Antuniassi, U. R., Correia, N. M. & Belapart, D. Manejo químico de plantas voluntárias de algodão rr. In *XXVIII Congresso Brasileiro da Ciência das Plantas Daninhas* (Sociedade Brasileira da Ciência das Plantas Daninhas, Campo Grande, Brasil, 2012).
7. Ikeda, F. S., Silva, C. P., Lima, R. S. & Oliveira, R. A. Comunidade de plantas daninhas e tiguera de algodão após a aplicação de herbicidas e adubação nitrogenada de cobertura em diferentes épocas no consórcio de milho com \*brachiaria ruziziensis\*. In *XXVII Congresso Brasileiro da Ciência das Plantas Daninhas* (Sociedade Brasileira da Ciência das Plantas Daninhas, Ribeirão Preto, Brasil, 2010). Accessed: 28/11/2024.
8. de Arruda, I. A. D. Manejo da destruição química da soqueira do algodoeiro no estado do mato grosso (2022).
9. Menin, T. Manejo de destruição de soqueira de algodão rr (2017).
10. Belot, J.-L. *Manual de Boas Práticas de Manejo do Algodoeiro em Mato Grosso*. Cuiabá, MT, 1ª edição edn. (2012). ISBN: 978-85-66457-00-1.
11. Wu, Z., Chen, Y., Zhao, B., Kang, X. & Ding, Y. Review of weed detection methods based on computer vision. *Sensors* **21**, 3647, [10.3390/s21113647](#) (2021).
12. Silva, J. A. O. S. *et al.* Deep learning for weed detection and segmentation in agricultural crops using images captured by an unmanned aerial vehicle. *Remote. Sens.* **16**, 4394, [10.3390/rs16234394](#) (2024).
13. C, S. G. *et al.* Field-based multispecies weed and crop detection using ground robots and advanced yolo models: A data and model-centric approach. *Smart Agric. Technol.* **9**, 100538, [10.1016/j.atech.2024.100538](#) (2024).
14. Champ, J. *et al.* Instance segmentation for the fine detection of crop and weed plants by precision agricultural robots. *Appl. Plant Sci.* **8**, e11373, [10.1002/aps3.11373](#) (2020). \_eprint: <https://onlinelibrary.wiley.com/doi/pdf/10.1002/aps3.11373>.

15. Czymmek, V., Harders, L. O., Knoll, F. J. & Hussmann, S. Vision-based deep learning approach for real-time detection of weeds in organic farming. In *2019 IEEE International Instrumentation and Measurement Technology Conference (I2MTC)*, 1–5 (IEEE, 2019).
16. Chen, D., Lu, Y., Li, Z. & Young, S. Performance evaluation of deep transfer learning on multi-class identification of common weed species in cotton production systems. *Comput. Electron. Agric.* **198**, 107091 (2022).
17. Yano, I. H., Alves, J. R., Santiago, W. E. & Mederos, B. J. Identification of weeds in sugarcane fields through images taken by uav and random forest classifier. *IFAC-PapersOnLine* **49**, 415–420 (2016).
18. Madec, S. *et al.* Vegann, vegetation annotation of multi-crop rgb images acquired under diverse conditions for segmentation. *Sci. Data* **10**, 302 (2023).
19. Genze, N. *et al.* Manually annotated and curated dataset of diverse weed species in maize and sorghum for computer vision. *Sci. Data* **11**, 109 (2024).
20. Champ, J. *et al.* Instance segmentation for the fine detection of crop and weed plants by precision agricultural robots. *Appl. Plant Sci.* **8**, e11373, <https://doi.org/10.1002/aps3.11373> (2020).
21. Minervini, M., Fischbach, A., Scharr, H. & Tsafaris, S. A. Finely-grained annotated datasets for image-based plant phenotyping. *Pattern Recognit. Lett.* **81**, 80–89, <https://doi.org/10.1016/j.patrec.2015.10.013> (2016).
22. Zenkl, R. *et al.* Outdoor plant segmentation with deep learning for high-throughput field phenotyping on a diverse wheat dataset. *Front. Plant Sci.* **12**, 774068, [10.3389/fpls.2021.774068](https://doi.org/10.3389/fpls.2021.774068) (2022).
23. Fan, X., Zhou, R., Tjahjadi, T., Choudhury, S. D. & Ye, Q. A segmentation-guided deep learning framework for leaf counting. *Front. Plant Sci.* **13**, 844522, [10.3389/fpls.2022.844522](https://doi.org/10.3389/fpls.2022.844522) (2022).
24. Woebbecke, D. M., Meyer, G. E., Von Bargen, K. & Mortensen, D. A. Color indices for weed identification under various soil, residue, and lighting conditions. *Transactions ASAE* **38**, 259–269 (1995).
25. Gongal, A., Amatya, S., Karkee, M., Zhang, Q. & Lewis, K. Sensors and systems for fruit detection and localization: A review. *Comput. Electron. Agric.* **116**, 8–19 (2015).
26. Corporation, C. Computer vision annotation tool (cvat), [10.5281/zenodo.4009388](https://doi.org/10.5281/zenodo.4009388) (2023).
27. Kirillov, A. *et al.* Segment anything. *arXiv:2304.02643* (2023).
28. Bradski, G. The OpenCV Library. *Dr. Dobb's J. Softw. Tools* (2000).
29. Jocher, G. & Qiu, J. Ultralytics yolo11 (2024).
30. Wang, A. *et al.* YOLOv10: Real-Time End-to-End Object Detection (2024). *ArXiv:2405.14458*.
31. Zhao, Y. *et al.* DETRs Beat YOLOs on Real-time Object Detection. In *2024 IEEE/CVF Conference on Computer Vision and Pattern Recognition (CVPR)*, 16965–16974, [10.1109/CVPR52733.2024.01605](https://doi.org/10.1109/CVPR52733.2024.01605) (IEEE, Seattle, WA, USA, 2024).
32. Pedregosa, F. *et al.* Scikit-learn: Machine learning in Python. *J. Mach. Learn. Res.* **12**, 2825–2830 (2011).
33. Liu, L. *et al.* Deep Learning for Generic Object Detection: A Survey, [10.48550/arXiv.1809.02165](https://doi.org/10.48550/arXiv.1809.02165) (2019). *ArXiv:1809.02165 [cs]*.
34. Bergstra, J., Yamins, D. & Cox, D. Making a science of model search: Hyperparameter optimization in hundreds of dimensions for vision architectures. In Dasgupta, S. & McAllester, D. (eds.) *Proceedings of the 30th International Conference on Machine Learning*, vol. 28 of *Proceedings of Machine Learning Research*, 115–123 (PMLR, Atlanta, Georgia, USA, 2013).
35. Watanabe, S. Tree-Structured Parzen Estimator: Understanding Its Algorithm Components and Their Roles for Better Empirical Performance, [10.48550/arXiv.2304.11127](https://doi.org/10.48550/arXiv.2304.11127) (2023). *ArXiv:2304.11127 [cs]*.
36. Ozaki, Y., Tanigaki, Y., Watanabe, S., Nomura, M. & Onishi, M. Multiobjective Tree-Structured Parzen Estimator. *J. Artif. Intell. Res.* **73**, 1209–1250, [10.1613/jair.1.13188](https://doi.org/10.1613/jair.1.13188) (2022).
37. Akiba, T., Sano, S., Yanase, T., Ohta, T. & Koyama, M. Optuna: A Next-generation Hyperparameter Optimization Framework, [10.48550/arXiv.1907.10902](https://doi.org/10.48550/arXiv.1907.10902) (2019). *ArXiv:1907.10902 [cs]*.
38. ClearML. Clearml - your entire mlops stack in one open-source tool (2024). Software available from <http://github.com/clearml/clearml>.
39. Kingma, D. P. & Ba, J. Adam: A Method for Stochastic Optimization, [10.48550/arXiv.1412.6980](https://doi.org/10.48550/arXiv.1412.6980) (2017). *ArXiv:1412.6980 [cs]*.
40. Virtanen, P. *et al.* SciPy 1.0: Fundamental Algorithms for Scientific Computing in Python. *Nat. Methods* **17**, 261–272, [10.1038/s41592-019-0686-2](https://doi.org/10.1038/s41592-019-0686-2) (2020).